Density of states of hole-doped manganites: A scanning-tunneling-microscopy/spectroscopy study

Amlan Biswas,* Suja Elizabeth, A. K. Raychaudhuri,† and H. L. Bhat
Department of Physics, Indian Institute of Science, Bangalore-560012, India
(Received 6 May 1998)

Variable temperature scanning-tunneling-microscopy/spectroscopy studies on single crystals and epitaxial thin films of hole-doped manganites, which show colossal magnetoresistance, have been done. We have investigated the variation of the density of states (DOS), at and near the Fermi energy (E_f), as a function of temperature. Simple calculations have been carried out, to find out the effect of temperature on the tunneling spectra and extract the variation of density of states with temperature, from the observed data. We also report here atomic resolution images, on the single crystals and larger range images showing the growth patterns on thin films. Our investigation shows unambiguously that there is a rapid variation in density of states for temperatures near the Curie temperature (T_c). While for temperatures below T_c, a finite DOS is observed at E_f, for temperatures near T_c a hard gap opens up in the density of states near E_f. For temperatures much higher than T_c, this gap most likely gives way to a soft gap. The observed hard gap for temperatures near T_c is somewhat higher than the transport gap for all the materials. For different materials, we find that the magnitude of the hard gap decreases as the T_c of the material increases and eventually, for materials with a T_c close to 400 K, the value of the gap approaches zero. [S0163-1829(99)11407-3]

I. INTRODUCTION

The phenomenon of colossal magnetoresistance (CMR) in hole-doped rare-earth manganites has, in recent times, been the subject of intense research efforts.[1–4] These oxides belong to the ABO_3 class of perovskite oxides and contain a mixed valency of Mn, which occupies the B site. The A site is occupied by rare-earth ions like Nd, La, etc. or by divalent ions like Pb, Ca, etc. These oxides, therefore, have the general formula $R_{1-x}M_xMnO_3$, where R is La, Nd, etc. and M is Ca, Pb, etc. There are a number of basic issues which need to be resolved to understand the unusual transport properties of these materials. One of the interesting properties is the sharp peak in resistivity (ρ) close to its ferromagnetic transition temperature (T_c). The peak in ρ is generally believed to arise from an insulator-metal-like transition on cooling below T_c. Since the system shows a transition from an insulatorlike state above T_c to a metallic state below T_c, it is likely that there is a change in the density of states (DOS) at the Fermi level (E_f), near T_c. The change in the DOS at $E_f[n(E_f)]$ is thus ushered in by changing the temperature. This issue is of fundamental importance as $n(E_f)$ will decide the nature of charge transport in the material. Questions like the existence of a gap in the DOS at E_f, localization of states near E_f, etc. are still unresolved. We formulate the following definite questions which we would like to seek answers to: (1) Is there a finite DOS at E_f below T_c, i.e., in the metallic state, and if so, does it have a temperature dependence? (2) Does a gap open up in the DOS near E_f above T_c, i.e., in the paramagnetic insulating state and if so is it temperature dependent?

In this paper we report our extensive investigations of the DOS of these materials as a function of temperature, using variable temperature scanning tunneling spectroscopy. We have carried out our studies on epitaxial thin films and single crystals of various compositions. Mainly we have studied two systems, namely, $La_{0.8}Ca_{0.2}MnO_3$ epitaxial thin films and single crystals of the system $La_{1-x}Pb_xMnO_3$.

II. EXPERIMENTAL DETAILS

Single crystals of $La_{1-x}Pb_xMnO_3$ were grown by the flux method using PbO and PbF_2 as solvents.[5] The flux ratio has been optimized to lower the growth temperature, to combat the high volatility of the flux. In addition, the heating, soaking, and cooling temperatures have been optimized. The precursors, homogenized in a ball mill, are transferred to a platinum-iridium crucible and closed tightly with a platinum lid. The growth process is carried out in a cylindrical resistive furnace, controlled by a programmable temperature controller. The charge is soaked at 1050 °C for 24 h and slow cooled in steps of several ramp rates ranging from 0.2 to 1.5 °C/h to 850° C, and thereafter furnace cooled to room temperature. Crystals of typical dimensions $1.5\times1.5\times1.5$ mm^3 are obtained by this method. The composition of the as-grown crystals is found by energy dispersive x-ray (EDX) analysis. The lead content is varied by changing the charge-to-flux ratio. Single crystals of the compound $(La_{1-y}Nd_y)_{1-x}Pb_xMnO_3$ are grown by a similar method [this compound will be, hereinafter, referred to as $(NdLa)_{1-x}Pb_xMnO_3$, which signifies that the Nd and La concentrations are $\sim(1-x)/2$, for the particular compound studied here]. La_2O_3, Nd_2O_3, and $MnCO_3$ are dissolved in the ratio 1:1:4 in the flux mixture of PbO-PbF_2 and crystal growth initiated as in the case of $La_{1-x}Pb_xMnO_3$. Here, crystals of typical dimension, $2.5\times2.5\times1.5$ mm^3, were obtained.

Epitaxial films of $La_{0.8}Ca_{0.2}MnO_3$ (referred as LCMO) were prepared by pulsed laser ablation on $LaAlO_3$ substrates, using the procedure described in Ref. 6.

The resistivities of the samples were measured by four-probe van der Pauw method (for the single crystals) or four-probe linear method (for the thin film). The magnetoresistance was measured using a superconducting solenoid.

Scanning tunneling microscopy/spectroscopy (STM/S) was done in a homemade variable temperature STM. The schematic diagram of the STM/S setup is shown in Fig. 1. The STM was operated from 100 K up to 375 K. During the

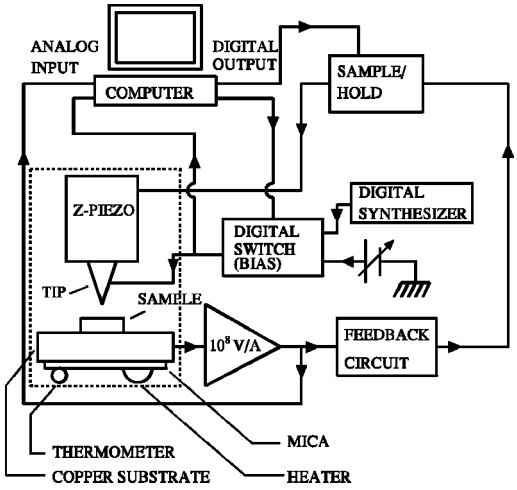

FIG. 1. A schematic representation of the STM/S setup. The dotted box indicates the STM head, which is kept in a cryopumped environment.

experiment the STM chamber is kept in a cryopumped environment and all other pumps are disconnected from the system.

Since we have operated our STM from temperatures up to 375 K and down to 100 K, we have chosen samples having a wide range of T_c to get data for a good range both above and below T_c. The single crystals' surfaces were scraped mechanically to expose a fresh surface before loading in the STM. The thin films were cleaned with methanol before loading in the STM chamber. Mechanically cut Pt-Rh(13%) tips were used for all the tunneling experiments. The samples were baked at about 370 K, in a vacuum of 5×10^{-6} torr, for 24 h prior to the STM/S measurements. The STM chamber was then cooled to liquid nitrogen temperatures and the chamber was isolated from the external pumps. The samples were further baked, at around 340 K, in a cryopumped environment for 5–6 h to avoid condensation of residual gases on the sample surface. The samples were then imaged at various magnifications and at different temperatures. The images obtained also served as a test of the cleanliness of the sample surface. The images were taken in the constant current mode, with the tip bias kept at 1.5 V and the tunneling current, during imaging, was stabilized at values ranging from 1 to 2 nA (exact values are specified for the particular images). Reproducible images were obtained over long durations indicating that the surfaces were stable and only after obtaining reproducible images was tunneling spectroscopy carried out. This ensured the cleanliness of the sample surface before the I-V spectra were recorded. We found that if gases like nitrogen are made to condense on the surface, most of the features in the I-V curves are washed out and the surface cannot be imaged. During data acquisition no external pumps were used and only the cryopump placed inside the chamber was used to retain the vacuum. Transport properties (e.g., resistivity) of the samples were measured before and after the tunneling experiments and no change in the properties was observed. This shows that there was no change in the oxygen content of the samples after the tunneling experiments, which were carried out in vacuum, as the transport properties depend critically on the oxygen content.

For recording the I-V spectra, the tip bias was kept at 1.5 V and the tunneling current (I_t) was stabilized at a particular value, with the feedback loop in the ''sample'' mode (see Fig. 1), i.e., the feedback signal to the z-piezo (Fig. 1) keeps the I_t (and hence the tip-sample distance) constant, for a constant tip bias. This is done to fix the tip-sample distance, i.e., the tunneling distance, at a particular value. The feedback was then put to ''hold'' mode by giving a digital signal to the sample/hold circuit, i.e., the value of the feedback signal was held constant and not allowed to change. This is done to prevent the feedback loop from changing the tip-sample distance when the tip bias is changed to obtain the I-V spectra. Thus, tunneling spectra, for constant tip-sample distance, can be obtained using this method. For details see Ref. 7. The tip bias was swept between $\pm$ 1 V at a frequency of 6 Hz and a set of I-V curves thus obtained were recorded digitally using a 16 bit analog to digital converter (ADC) card. The gain of the current amplifier is 10^8 V/A and the resolution of the ADC card is 300 μV, so the minimum measurable current with this setup is about 3 pA. The data were recorded at a rate of 7.2 KHz. A set of 5 I-V curves was averaged. The dI/dV-V and $d\ln I/d\ln V$-V curves were obtained by numerical differentiation of such average I-V curves. This procedure was repeated for different values of stabilization currents and at different points on the sample surface, at each temperature.

To determine the exact value of the gaps observed, variable distance tunneling measurements were carried out for one sample $[(NdLa)_{0.73}Pb_{0.27}MnO_3]$. This was done only for positive tip bias (filled states of the sample). The procedure followed was the same as above except the tip bias was swept from 0.01 to 2 V instead of $\pm$1 V and the feedback was kept in the sample mode. With an active feedback loop the tip went closer to the sample for lower biases, in order to keep the I_t constant. This gave us a large dynamic range for the measurement of I_t and we were able to measure the correct voltage value for which the I_t goes to zero and hence the correct energy value for the band edges. For details of this method see Ref. 8.

III. RESULTS

In Fig. 2 we show the resistivity data of the samples studied. The materials, as expected, show a peak in ρ at a temperature close to T_c. We designate this temperature, where the peak in ρ occurs, as T_{IM} (IM denotes insulator to metal). The resistivities of the single crystals are much less than that of the thin film. However, due to the small size of the crystals, the absolute values of ρ have uncertainties. The details of the samples are given in Table I. Some of the quantities were not measured due to experimental limitations, but the essential quantities for our subsequent analyses and conclusions have been measured. The resistivities are shown in zero field or in an applied field (3 or 6 T). For the LCMO film the maximum magnetoresistance (MR) is in excess of 80% for an applied field of 6 T. For $(NdLa)_{0.73}Pb_{0.27}MnO_3$ the maximum MR (at 3 T) is nearly 70%. Here we have defined the MR as $[\rho(0)-\rho(H)]/\rho(0)$. It can be seen from the data on the $(NdLa)_{0.73}Pb_{0.27}MnO_3$ system that the T_c and T_{IM} can be varied over a large temperature range by substituting Nd in place of La. This is expected, because the T_c, in these materials, decreases as the average A-site cation radius ($\langle r_A\rangle$) decreases. Here A site refers to the A site of the ABO_3 struc-

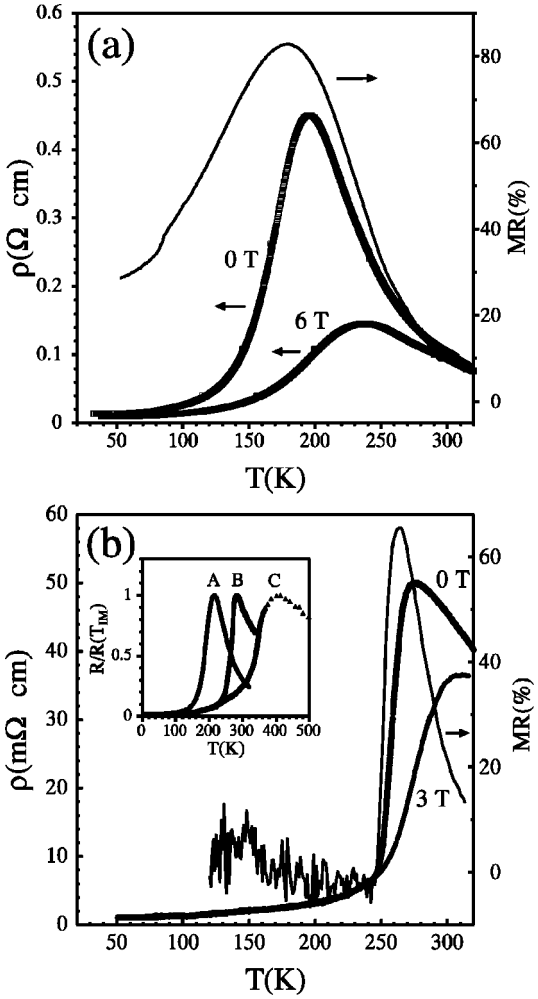

FIG. 2. (a) The resistivity and magnetoresistance of the LCMO epitaxial thin film. (b) The resistivity and magnetoresistance of the $(NdLa)_{0.73}Pb_{0.27}MnO_3$ single crystal. The inset shows the scaled resistivities of three of the samples studied, (A) LCMO thin film, (B) $(NdLa)_{0.73}Pb_{0.27}MnO_3$ single crystal, (C) $La_{0.6}Pb_{0.4}MnO_3$, showing the variation in T_{IM}.

ture. Substitution of smaller Nd in place of La thus leads to the reduction of T_c.[9,10]

Figure 3 shows an atomic resolution image obtained for the sample $La_{0.6}Pb_{0.4}MnO_3$. The distance between the brighter spots is 4.02 ± 0.2 Å as derived from our calibration done on graphite. These materials have a pseudocubic structure and the unit cell is nearly cubic or rhombohedral with $\alpha \approx 60.52°$ (for a perfect cube, $\alpha = 60°$), as obtained from x-ray structure determination. The Mn-O-Mn distance in these materials is around 3.87 Å. The distance observed by us is thus close to this distance and the difference can arise due to the uncertainty in calibration. One may thus argue that the surface exposed has Mn-O-Mn chains. However, we have not been able to ascertain, unambiguously, the chemical identity of the imaged atoms. To determine the chemical identity of the atoms, further studies involving bias dependent imaging of the surface have to be performed. We also observe a distortion from the perfect square array, as can be seen from the 4.02 Å $\times$ 4.02 Å parallelogram drawn in Fig. 3.

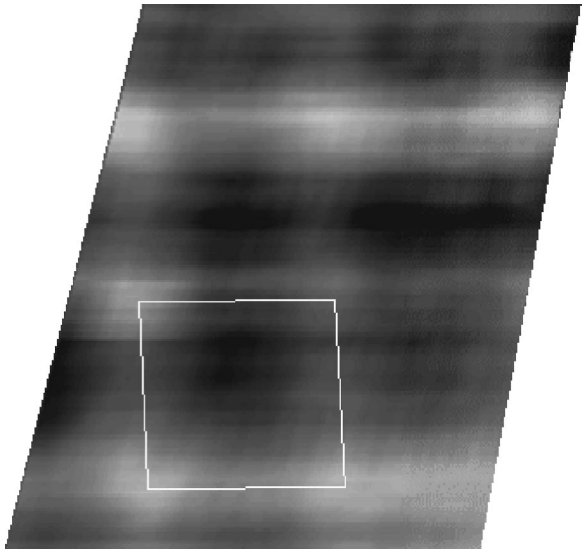

FIG. 3. Atomic resolution image of $La_{0.6}Pb_{0.4}MnO_3$ single crystal. The image was taken in the constant current mode, with a tip bias of +1.5 V and a tunneling current of 1.2 nA. The temperature of the sample was 320 K. The parallelogram indicates a cell of size 4.02×4.02 Å.

Figure 4 shows an 853 Å $\times$ 906 Å image of the LCMO thin film. This image shows atomically smooth terraces, which end in atomic level steps as marked by the arrows.

TABLE I. The details of the samples studied. The Curie temperature (T_c), the temperature where the peak in ρ occurs (T_{IM}), the transport activation gap (E_a), the maximum value of the gap in the DOS near E_f for $T \approx T_c$, measured by tunneling spectroscopy ($2\Delta_{max}$), and the temperature where the gap in the DOS opens while heating the sample from much below T_c(T_{gap}) are shown, for the different samples. Some of the values could not be measured due to experimental limitations.

Sample	Type	T_c (K)	T_{IM} (K)	E_a (eV)	$2\Delta_{max}$ (eV)	T_{gap} (K)
$La_{0.8}Ca_{0.2}MnO_3$	epitaxial thin film		196	0.121	0.215	178
$(NdLa)_{0.73}Pb_{0.27}MnO_3$	single crystal	290	275	0.052	0.156	254
$La_{0.7}Pb_{0.3}MnO_3$	single crystal	338			0.059	325
$La_{0.6}Pb_{0.4}MnO_3$	single crystal		401	0.041		

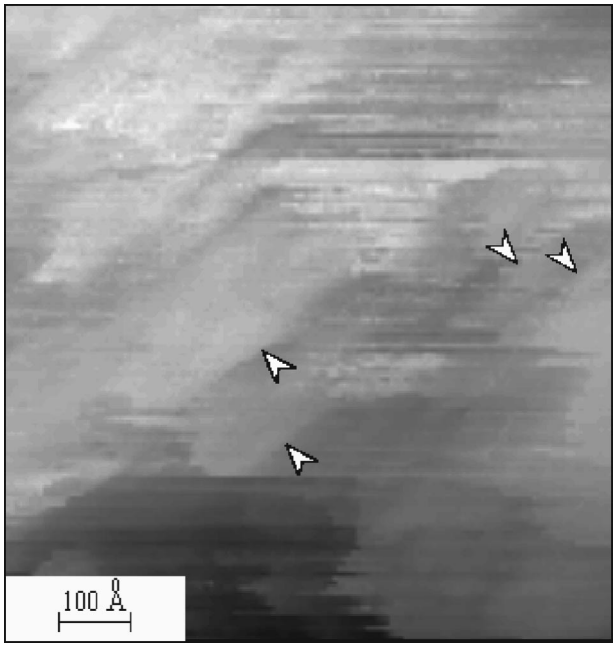

FIG. 4. An 853 Å $\times$906 Å image of the LCMO thin film. The image was taken in the constant current mode, with a tip bias of +1.5 V and a tunneling current of 2 nA. The temperature of the sample was 298 K. The atomically smooth terraces are terminated by atomic steps, some of which are marked by the arrows.

These are typical growth patterns often observed in thin film samples of these oxides.[11,17]

Figure 5 shows the dI/dV-V (G-V) curves for two of the samples, $La_{0.7}Pb_{0.3}MnO_3$ single crystal and LCMO thin film. In our subsequent discussions we have referred to these curves. We have shown the data for three distinct regions, $T<T_c$, $T\approx T_c$, and $T>T_c$. To avoid overcrowding of data, we have shown only a cross section of the data taken.

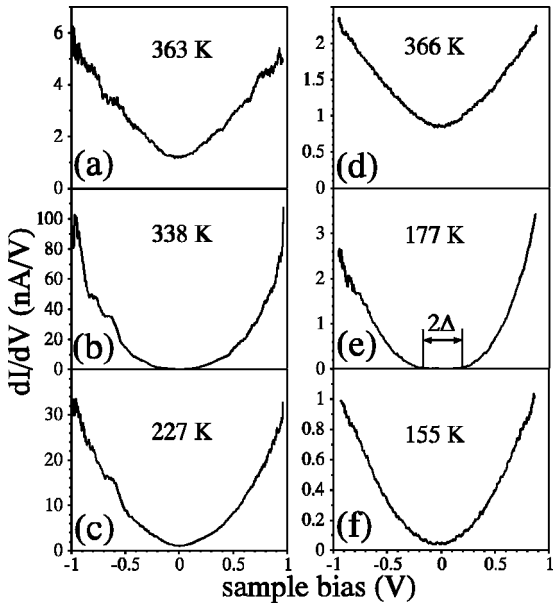

FIG. 5. G-V curves at different temperatures for (a), (b), and (c) $La_{0.7}Pb_{0.3}MnO_3$ single crystal and (d), (e), and (f) LCMO thin film. The gap observed for $T\approx T_c$, i.e., 2Δ, is shown for the LCMO sample.

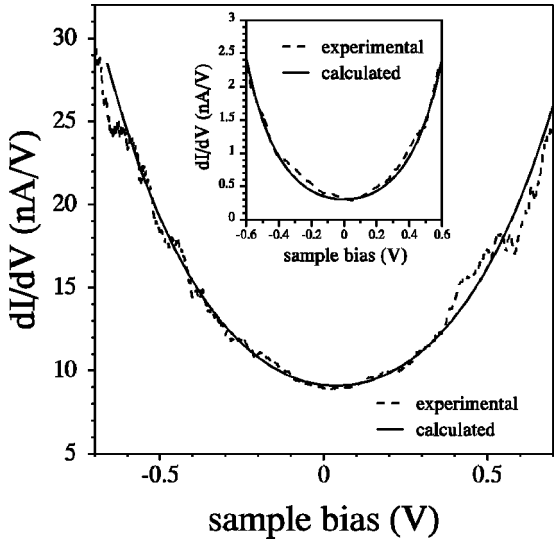

FIG. 6. G-V curve for 500 Å platinum film, at 307 K. The solid line is the calculated G-V curve (described in text). The inset shows the G-V curve for the same film at 134 K. The solid line is the calculated G-V curve.

The G-V curves, for all the samples, show qualitative variations with temperature, when the temperature is changed across the T_c. This is obvious directly from the G-V curves. Before a detailed discussion of the results, we point out some preliminary observations which can be made from the G-V curves shown above, which are common to all the samples studied. For $T<T_c$, the G-V curves [Figs. 5(c) and 5(f)] resemble those for a good metal, like platinum. There is a finite value of the zero-bias conductance (G_0), and the G-V curves are parabolic. The parabolic nature of the G-V curves is essentially a property of the tunneling barrier.[16] This is expected as the metallic state is stabilized below T_c. For comparison we show, in Fig. 6, the G-V curve for a 500 Å film of platinum at 307 K. The inset shows the G-V curve for the same film at 134 K. The calculated curves shown in the figure are discussed later in Sec. IV B. The film was grown on a fire-polished glass surface using electron-beam evaporation, in a base pressure of 10^{-8} torr.

As the temperature is increased to $T\approx T_c$, G_0 goes to zero and a gaplike feature opens up near zero bias, i.e., the Fermi level [Figs. 5(b) and 5(e)]. As the temperature is increased further to $T>T_c$, G_0 becomes nonzero again and the gaplike feature vanishes [Figs. 5(a) and 5(d)]. But these G-V curves are qualitatively different from the metal-like G-V curves for $T<T_c$. We will see below that this particular feature of the tunneling data for $T>T_c$ implies the existence of a soft gap near E_f, with additional contributions to G_0 arising due to finite temperature.

IV. DISCUSSION

The tunneling spectroscopy data as presented in the preceding section need to be analyzed quantitatively before further conclusions can be drawn from them. There are different recipes for obtaining the density of states from tunneling data.[12–14] However, the problem becomes involved if the DOS itself is temperature dependent. This is in addition to the temperature dependence which arises through the Fermi

function $f(E,T)$. In the following, we have tried to take into account all these effects to derive certain quantitative conclusions about the DOS. We have arranged the following discussion in four subsections, to analyze our data, so that quantitative information about the DOS $[n(E)]$ can be obtained to the extent possible. In the first section we analyze the data for energy $|E-E_f| \geqslant 0.2$ eV which is the region away from E_f so that the overall temperature dependence of $n(E)$ can be obtained. In the second section we analyze the $n(E)$ near the E_f for the ferromagnetic region ($T<T_c$). In the third section we analyze the data for temperatures near the transition temperature T_c($T \approx T_c$). In the fourth section we have investigated the region close to E_f, for the paramagnetic regime ($T>T_c$).

A. DOS for $|E\text{-}E_f| \geqslant 0.2$ eV

In this section we discuss the features in the DOS for $|E-E_f| \geqslant 0.2$ eV. Figure 7 shows the $d\ln I/d\ln V$-V curves for different temperatures, for some of the samples studied. $d\ln I/d\ln V$ is the normalized conductivity $(dI/dV)/(I/V)$. This quantity is generally used as a measure of the DOS, independent of the barrier parameters.[13] The division of the differential conductance (dI/dV) by I/V reduces the effect of the barrier parameters. Within certain limits $d\ln I/d\ln V$ does give a measure of the DOS.[12] This quantity $(d\ln I/d\ln V)$ is not well defined near zero bias, when there is a gaplike feature in the DOS (low G_0) near the Fermi level.[15] Due to this limitation we have calculated $d\ln I/d\ln V$ outside the region of very low $G_0(|V| \geqslant 0.2$ V) from the observed data. The tunneling spectra for the low-bias region will be discussed in the following sections. From Fig. 7 we conclude that the DOS for $|E-E_f| \geqslant 0.2$ eV changes dramatically with temperature, when the temperature is changed across T_c. The behavior shown in Fig. 7(a) is a typical example. For $T<T_c$, the DOS has a stronger dependence on energy, on both the filled ($V<0$) and unfilled ($V>0$) side than that for $T>T_c$. Also the temperature dependence of $(d\ln I/d\ln V)$ saturates for $T/T_c < 0.75$, as shown in the inset of Fig. 7(b) where we have shown an example for $La_{0.6}Pb_{0.4}MnO_3$, which has a $T_c > 400$ K (we could not measure T_c due to experimental limitations; however, the $T_{IM}=401$ K).

The temperature variation of $(d\ln I/d\ln V)$ at a given voltage $V=0.9$ V$[(d\ln I/d\ln V)_{0.9\text{ V}}]$ is shown in Fig. 8 to find out the extent of variation in $(d\ln I/d\ln V)$. We have chosen $V=0.9$ V, as it is away from $V=0$ and thus represents states away from E_f. It can be seen from Fig. 8 that $(d\ln I/d\ln V)_{0.9\text{ V}}$ is higher for $T<T_c$ than that for $T>T_c$ (a preliminary observation has been reported in Ref. 12 and similar observations have been reported in Ref. 17). This implies that the DOS is higher in value for $T<T_c$, in this energy range, and it has a distinct temperature variation as T changes through T_c. Eventually, for $T \ll T_c$, a temperature independent value is obtained. This was seen before in the inset of Fig. 7(b). The behavior seen in Fig. 8 has two noteworthy features. First, there is a distinct peak in $(d\ln I/d\ln V)_{0.9\text{ V}}$ at $T \approx T_c$. This is seen in all the samples. Second, the peak is sharper for the single crystal than for the thin film.

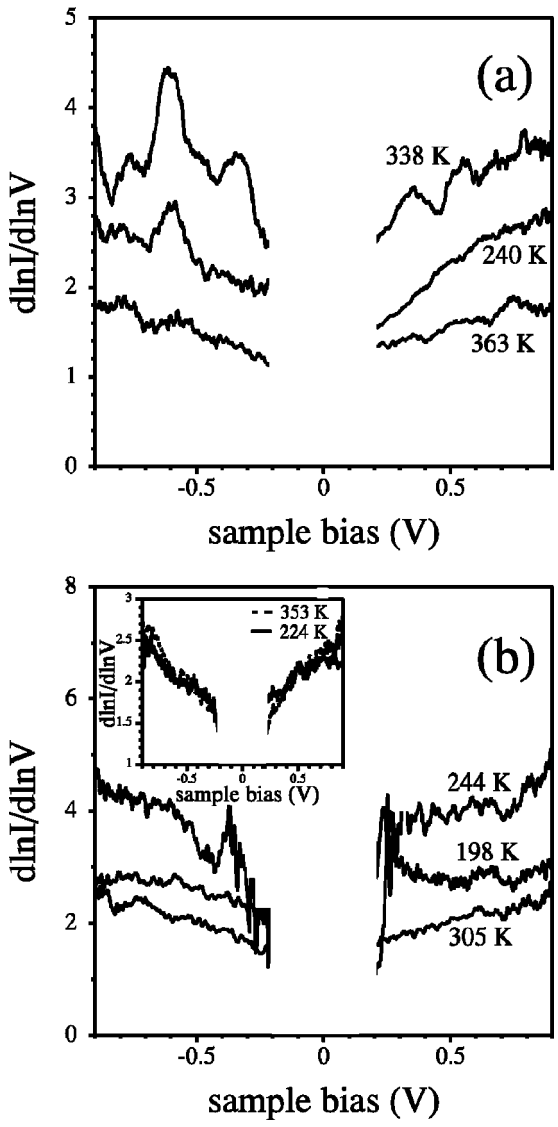

FIG. 7. $d\ln I/d\ln V$-V curves for $|V| \geqslant 0.2$ V at different temperatures for (a) $La_{0.7}Pb_{0.3}MnO_3$($T_c=338$ K), (b) $(NdLa)_{0.73}Pb_{0.27}MnO_3$ ($T_{IM}=275$ K). The inset in (b) shows the $d\ln I/d\ln V$-V curves at two temperatures for $La_{0.6}Pb_{0.4}MnO_3$ ($T_{IM}=401$ K), which illustrates that for temperatures well below T_{IM}, there is no appreciable change in the DOS with temperature.

For $T \approx T_c$, a gaplike feature is present in the DOS near E_f and this results in a very sharp increase in the DOS beyond a particular voltage. This is seen in Fig. 8 as a rapid increase of $(d\ln I/d\ln V)_{0.9\text{ V}}$, close to T_c. The increase in DOS at higher energies (away from E_f), in the temperature range close to T_c where there is a gap at E_f, may imply a transfer of relative spectral weights to higher energies when the gap opens up.

B. Tunneling data for $T<T_c$

For $T<T_c$, there is a finite tunneling conductance at zero bias, G_0. This is expected since, for $T<T_c$, the metallic state is stabilized and so we conclude that there is a finite DOS at $E_f[n(E_f)]$. However, G_0 also depends on the barrier parameters of the tunnel junction formed between the tip and sample, in addition to $n(E_f)$ and the temperature. For tun-

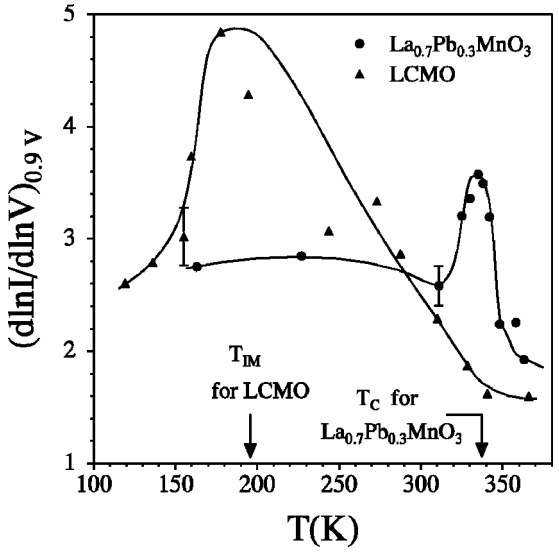

FIG. 8. A plot of the quantity $(d\ln I/d\ln V)_{0.9\ \mathrm{V}}$ vs T for two samples, showing the redistribution of spectral weight with temperature. The solid lines are guides to the eye and typical error bars are shown.

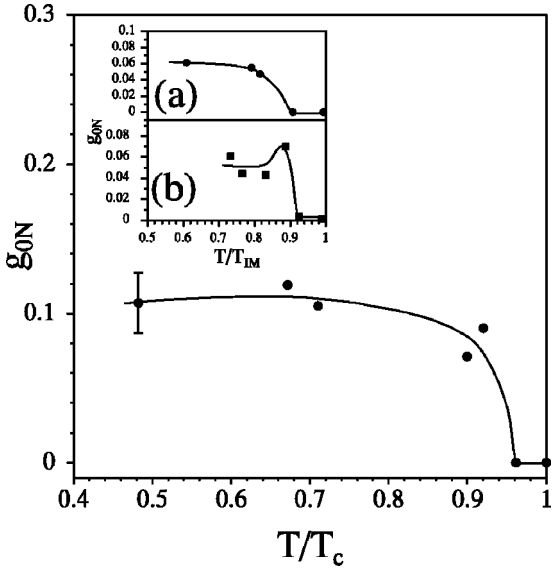

FIG. 9. The g_{0N} vs T/T_c plot for $La_{0.7}Pb_{0.3}MnO_3$, showing that $n(E_f)$ drops to zero just below T_c, when the temperature is increased from below T_c. A typical error bar is shown. The inset shows the g_{0N} vs T/T_{IM} plots for the samples (a) LCMO thin film and (b) $(NdLa)_{0.73}Pb_{0.27}MnO_3$ single crystal. The solid lines are guides to the eye.

neling spectroscopy done at variable temperature it is difficult to ensure the constancy of these parameters. The usual normalization procedures which remove the effect of the barrier parameters do not describe the region near zero bias (i.e., near E_f) satisfactorily. To remove this dependence on the barrier parameters and also get an estimate of the relative change of $n(E_f)$ with temperature, we normalize G_0 by the tunneling conductance at 0.9 V ($G_{0.9}$). But $G_{0.9}$ itself might have a temperature dependence due to the change in DOS with temperature at that energy. We expect that the variation of $G_0/G_{0.9}$, due to the variation of $G_{0.9}$, can be accounted for if the observed temperature dependence of $G_{0.9}$ itself is taken care of by some normalization factor which is independent of the barrier parameters and depends only on the DOS at that energy. Therefore, we plot the quantity

$$g_{0N}(T)=\frac{G_0(T)}{G_{0.9}(T)}\left(\frac{d\ln I}{d\ln V}\right)_{0.9\ \mathrm{V},T}, \tag{1}$$

where $(d\ln I/d\ln V)_{0.9\ \mathrm{V},T}$ is the value of $d\ln I/d\ln V$ at a sample bias of 0.9 V and at a temperature T. This quantity is known experimentally and it is independent of the barrier parameters and depends only on the DOS at that particular energy at a temperature T. This normalized ratio $g_{0N}(T)$ in Eq. (1) is thus expected to mostly reflect the variation arising from the temperature variation of $n(E_f)$. The plots of g_{0N} for three different samples are shown in Fig. 9. For all the samples $g_{0N}(T)$ shows a rise below T_c (or T_{IM}) as the material enters the metallic state and it reaches a temperature independent value at lower temperatures. For the epitaxial film the growth of g_{0N} [and hence of $n(E_f)$] is gradual whereas for the single crystals this rise is rather sharp. *These observations would imply that $n(E_f)$ grows rapidly below T_c and reaches a temperature independent value, as in a metal. This is a very important conclusion of our experiment.*

The observed parabolic shape of the G-V curves and the fact that $g_{0N}(T)$ has a negligible dependence on temperature below T_c indicate that the DOS near E_f is flat in the scale of k_BT and temperature independent below T_c, just like a metal. To strengthen this conclusion, quantitatively, we carried out a simple calculation using the expression for tunneling current given below and a constant DOS for both tip and sample. Equation (2) gives the expression for the tunneling current for a trapezoidal barrier[16,12]:

$$\begin{aligned} I(s,V,W,T)=c\int_{-\infty}^{\infty}&N_s\left(E+\frac{eV}{2}\right)N_t\left(E-\frac{eV}{2}\right)\\ &\times\left[f\left(E-\frac{eV}{2},T\right)-f\left(E+\frac{eV}{2},T\right)\right]\\ &\times\tilde{t}(s,E,W)dE, \end{aligned} \tag{2}$$

where the barrier penetration factor $\tilde{t}$ is given by

$$\tilde{t}(s,E,W)=\exp[-2ks\sqrt{2(W-E)}], \tag{3}$$

where E is the energy of the electron, c is a constant dependent on the tip-sample effective junction area, s is the tip-sample distance, W is the average work function of the tip and sample surface, V is the bias between tip and sample, T is the temperature, $N_t(E)$ and $N_s(E)$ are the tip and sample DOS, respectively, $k=\sqrt{m}/\hbar$ (m is the electron mass), and $f(E,T)$ is the Fermi function at temperature T. In the above expression all the energies are measured with respect to E_f which is the zero of the energy scale.

Figure 10(a) shows a comparison between an experimental G-V curve, taken on the LCMO thin film at 160 K ($T<T_c$), and a calculated G-V curve using constant tip and sample DOS, a tip-sample distance of 6.5 Å , and a work function of 1.2 eV. The good agreement between the observed data and the calculated curves supports our conclusion that below T_c, the DOS near and at E_f is finite and metal-like. For comparison, the experimental and calculated

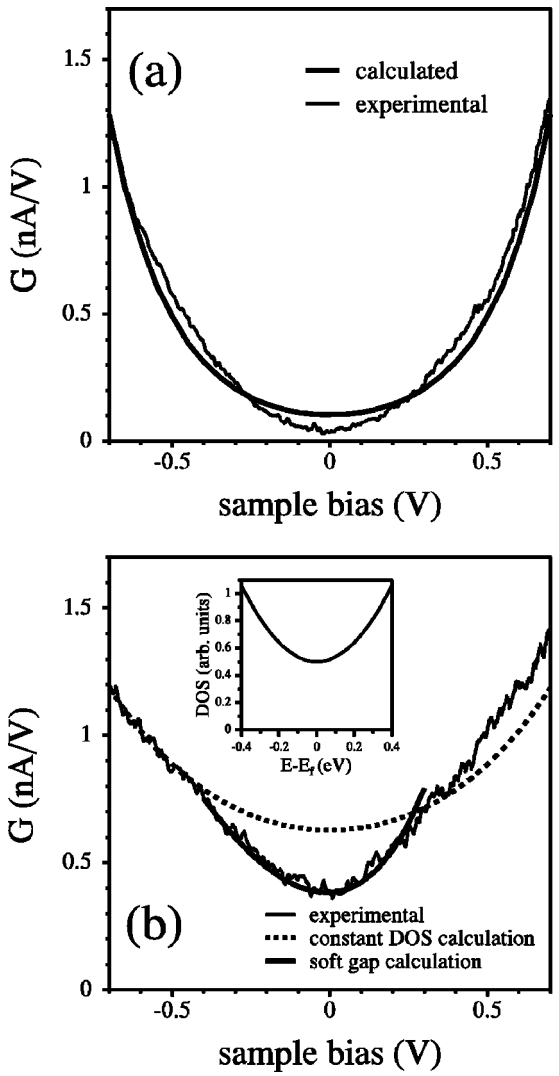

FIG. 10. A comparison of the experimental and calculated G-V curves for the LCMO thin film. (a) The sample temperature is 160 K. (b) The sample temperature is 328 K, the dashed line showing the constant DOS calculation and the thick solid line showing the model DOS calculation. The inset in (b) shows the model DOS used to calculate the G-V curve for the bias range $|V|<0.4$ V, for $T=328$ K.

G-V curves [using again a constant tip and sample DOS and Eq. (2)] for a 500 Å platinum film are shown in Fig. 6.

The change in conductivity (σ) below T_c will arise from a change in the mobility (μ) and/or a change in the carrier concentration (N) [$\sigma=Ne\mu$]. The increase in μ below T_c is expected due to the suppression of the spin disorder scattering as the local magnetization builds up. However, if $n(E_f)$ rises rapidly below T_c, and builds up from a zero value at T_c, it is expected that the effective carrier concentration N also rises as the sample is cooled below T_c. *The large variation in ρ near T_c may be a consequence largely of a variable $n(E_f)$, giving rise to a large variation in N, with a lesser contribution coming from the temperature dependent mobility $\mu(T)$.*

C. Tunneling data for $T\approx T_c$

For $T\approx T_c$, the value of G_0 goes to zero and a gap opens up in $n(E)$ near E_f, as is evident from the G-V curves shown in Fig. 5 and the plot of g_{0N} vs T shown in Fig. 9. The gap (2Δ) is shown for one G-V curve in Fig. 5. On heating from below T_c this gap opens at $\sim$15–20 K below T_{IM} (or T_c) and sharply rises to the maximum value. We denote the temperature where the gap opens as $T_{\rm gap}$. It then decreases in magnitude as the temperature is increased further above T_c and finally disappears as the temperature is increased well beyond T_c and the observed G_0 becomes nonzero. These observations would indicate that close to T_c a gap develops in the DOS near E_f. This gap collapses as the sample is cooled below T_c. The nature of the DOS near E_f for $T\gg T_c$ will be discussed later.

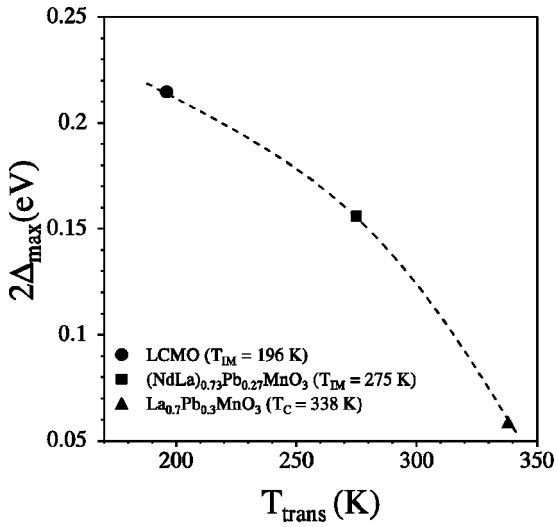

FIG. 11. A plot of the maximum value of the tunneling gap ($2\Delta_{\rm max}$) vs $T_{\rm trans}$, where $T_{\rm trans}$ is either T_c or T_{IM}, as specified in the figure. The dotted line is a guide to the eye.

These features are observable both in the epitaxial film and single crystals. However, the transitions are sharper for the single crystals. There is also a very interesting similarity between $T_{\rm gap}$ and the temperature where the MR of the material shows a peak. It will be interesting to see if such large MR actually arises due to such drastic changes in DOS on the application of a magnetic field, when the sample temperature is near T_c. In Fig. 11 the maximum values of the gaps ($2\Delta_{\rm max}$) observed in different materials have been plotted against the T_c (or T_{IM}) of the materials. It is clear that the observed $2\Delta_{\rm max}$ has a strong correlation with the T_c. The T_c's of these materials are related to the bandwidths (the width of the Jahn-Teller split e_g bands). *A material with larger bandwidth has a larger T_c. The decrease in $2\Delta_{max}$ as T_c increases would imply that $2\Delta_{max}$ decreases as the bandwidth increases. This is an important conclusion.* This also shows that any mechanism that can change the bandwidth will change the value of $2\Delta_{\rm max}$ and hence the transport properties close to T_c. Eventually, for $T_c\rightarrow 400$ K (as in materials like $La_{0.7}Sr_{0.3}MnO_3$) the gap is expected to reduce to extremely small values. Interestingly, the largest T_c observed in these materials is around 400–450 K. These values of the gaps, measured by tunneling, are comparable to the transport activation gap in these materials, as estimated from the ρ vs T data, which are $\sim$0.1 eV (see Table I).

To verify that the gap is real, i.e., the current actually goes to zero within the gap region, we carried out variable sepa-

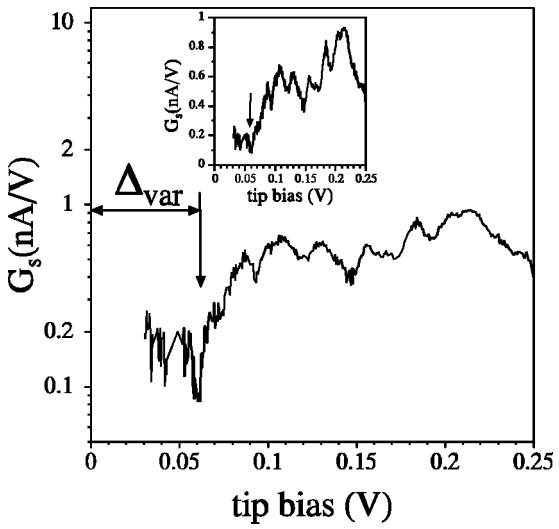

FIG. 12. Variable distance G_s-V curves for the sample $(NdLa)_{0.73}Pb_{0.27}MnO_3$, at a temperature 270 K. The gap Δ_{var} is indicated by the arrows. The G_s scale is logarithmic. The inset shows the same curve with a linear G_s scale and the gap Δ_{var} is marked by the arrow.

ration tunneling spectroscopy, as described in detail in Ref. 8. In this technique, the tip is brought closer to the sample as the bias between the tip and sample and consequently I_t approaches zero (the particular method used is described briefly in Sec. II). This gives a high dynamic range in the measurement of the tunneling current. This method enables us to effectively measure tunneling currents over a few orders of magnitude, so that we can properly define the band edges. Although we have not converted the variable distance measurements to constant distance measurements, our purpose, of verifying the band edges, is still served from just the as-acquired data. This experiment was done only for positive tip bias, i.e., for the filled states of the sample. Therefore we were able to observe the band edge only for the filled states of the sample. Figure 12 shows the variable distance conductance (G_s) data, and it shows the gap feature, denoted by Δ_{var}, just like the constant distance tunneling data. The experiment was done at 270 K and the values of Δ_{var} and Δ (at $T \approx 270$ K) agree to within 0.01 eV. This combination of the two techniques gives a quantitative foundation to the observed gap.

D. Tunneling data for $T > T_c$

Above T_c, the gap near E_f closes again and G_0 assumes a finite value. This implies, essentially, appearance of finite DOS at E_f. However, the transport in the material is still activated. This is possible only if the new states arising close to E_f are localized. We have to interpret our tunneling data carefully since, at such high temperatures, the temperature itself plays an important role in determining the shape of the G-V curves. However, we have carried out numerical calculations again using Eq. (2), to find out if the observed disappearance of the gap at high temperatures is due to the thermal smearing of the tunneling spectra, and *have found that the disappearance of the gap cannot be explained due to the thermal smearing alone*. In order to explain our tunneling data for $T > T_c$ we have to make the following proposition. We propose that the gap which developed near E_f for $T \approx T_c$ collapses to a soft, Coulomb gap for $T > T_c$. The presence of a soft, Coulomb gap suggests that the states around E_f are localized. One then has an interplay of Coulomb interaction and disorder. However, further investigation is required before issues like the existence of a Coulomb gap can be established beyond doubt. At this moment we can only state that using the above model, we can fit our data quantitatively. However, we cannot guarantee that this is the only way to explain the data. In the following, we describe the model calculations which were carried out to determine the nature of the DOS for $T > T_c$.

In Fig. 10(b), we show the comparison of the experimental G-V curve taken at 328 K (i.e., for $T \gg T_c$) for the LCMO thin film sample, with the calculated G-V curves [using Eq. (2)] at that temperature. The dotted line shows the calculated curve using a constant DOS for the tip and sample. The tunneling distance and the work function were taken as 2.5 Å and 1.2 eV, respectively. This can be taken as the background voltage dependence of G for the tunnel junction, due to just the barrier parameters, s and W. But unlike for $T < T_c$, the measured G-V curve dips below the calculated constant DOS curve for $|V| < 0.4$ V, therefore suggesting that there is a dip in the DOS near the Fermi level for $|E - E_f| < 0.4$ eV. Also, there is a significant asymmetry in the measured G-V curve. We have calculated the G-V curve using the model DOS, shown in the inset of Fig. 10(b), for the sample and a constant DOS for the tip in Eq. (2) and the same barrier parameters used for the constant DOS calculation, for the bias region $|V| < 0.4$. The model DOS is taken as a quadratic function of $|E - E_f|$. The value of the model DOS is nonzero at E_f (which was required for a good match with our experimental data), unlike a Coulomb gap. This could be due to the fact that the DOS, in the presence of a Coulomb gap, has an explicit temperature dependence which results in a change in the width of the Coulomb gap as well as a nonzero value for the DOS at E_f, at such high temperatures.[18] The calculated G-V curve using this model DOS is shown as the solid line in Fig. 10(b). It is interesting to note that the tunneling distance estimated from the G-V curves for $T < T_c$ (about 6.5 Å) is much larger than that estimated from the G-V curves for $T > T_c$ (about 2.5 Å). This could again be a consequence of the fact that the states near E_f are localized for $T > T_c$. The asymmetry in the experimental G-V curves for $T > T_c$ is reproduced, to a certain extent, by our calculation using the model DOS. Therefore from the analysis given above we conclude that for $T > T_c$ a Coulomb (soft) gap is formed at E_f.

To summarize, our experiment suggests that the hard gap existing close to T_c closes at a temperature somewhat higher than T_c and gives way to a soft gap with localized states near E_f. This is an important observation. However, more experiments are needed to confirm the above picture.

V. SUMMARY AND CONCLUSION

From the tunneling studies carried out and the discussion in the above sections, it is clear that the density of states of hole-doped manganites shows large changes near E_f, when the temperature is changed across T_c. This plays an important role in determining the transport properties, like resis-

tance and magnetoresistance, of these materials. When the temperature is changed across T_c, there is a transfer of spectral weight in the DOS. Below T_c the metallic state is stabilized and there is a finite DOS near E_f, which is flat in the scale of k_BT.

When the temperature is increased from below T_c, a gap appears in the DOS near E_f, just below T_c. The value of this gap is comparable to the transport gap, estimated from the resistivity data above T_c. The maximum value of this gap is higher for the samples with lower T_c. It may happen that, if near T_c the applied magnetic field modifies this feature of the DOS near E_f, then this will be reflected as a large change in ρ and can thus be the origin of CMR in these materials. Our experiment suggests that, on heating much above T_c, the hard gap gives way to a soft gap near E_f, indicating that the states near E_f are localized. Opening up of a hard gap can arise from the Jahn-Teller effect whereas a soft gap arises from Coulomb interactions for localized states. Our data suggest that there is a presence of both these factors above T_c, modifying the nature of DOS.

ACKNOWLEDGMENTS

This work is supported by CSIR, Government of India. The authors would like to thank Professor C.N.R. Rao and Professor T.V. Ramakrishnan for helpful discussions.

*Present address: Center for Superconductivity Research, Department of Physics, University of Maryland, College Park, Maryland 20742.

†Present address: National Physical Laboratory, Dr. K.S. Krishnan Marg, New Delhi-110012, India.

[1] R. von Helmolt, J. Wecker, B. Holzapfel, L. Schultz, and K. Samwer, Phys. Rev. Lett. **71**, 2331 (1993).

[2] K. Chahara, T. Ohno, M. Kasai, and Y. Kozono, Appl. Phys. Lett. **63**, 1990 (1993).

[3] A. Urushibara, Y. Moritomo, T. Arima, A. Asamitsu, G. Kido, and Y. Tokura, Phys. Rev. B **51**, 14 103 (1995).

[4] R. Mahendiran, R. Mahesh, A. K. Raychaudhuri, and C. N. R. Rao, J. Phys. D **28**, 1743 (1995).

[5] A. H. Morrish, B. J. Evans, J. A. Eaton, and L. K. Leung, Can. J. Phys. **47**, 2691 (1969).

[6] M. Rajeswari *et al.*, Appl. Phys. Lett. **69**, 851 (1996).

[7] J. A. Stroscio and W. J. Kaiser, *Scanning Tunneling Microscopy* (Academic Press, San Diego, CA, 1993).

[8] C. K. Shih, R. M. Feenstra, and G. V. Chandrashekhar, Phys. Rev. B **43**, 7913 (1991).

[9] H. Y. Hwang, S.-W. Cheong, P. G. Radaelli, M. Marezio, and B. Batlogg, Phys. Rev. Lett. **75**, 914 (1995).

[10] R. Mahesh, R. Mahendiran, A. K. Raychaudhuri, and C. N. R. Rao, J. Solid State Chem. **120**, 204 (1995).

[11] Geetha Ramaswamy and A. K. Raychaudhuri, J. Appl. Phys. **80**, 4519 (1996).

[12] Amlan Biswas and A. K. Raychaudhuri, J. Phys.: Condens. Matter **8**, L739 (1996).

[13] J. A. Stroscio, R. M. Feenstra, and A. P. Fein, Phys. Rev. Lett. **57**, 2579 (1986).

[14] Vladimir A. Ukraintsev, Phys. Rev. B **53**, 11 176 (1996).

[15] One can calculate the quantity $(dI/dV)/(\overline{I/V})$ instead of $(d\ln I/d\ln V)$, when there is a gaplike feature in the DOS near E_f. $\overline{I/V}$ is calculated numerically from I/V by using a weighting function and a spectral width of the order of the gap (Ref. 17). Division of dI/dV by $\overline{I/V}$ instead of I/V smooths out the numerical divergences near zero bias. But this procedure also removes information from the region near zero bias, which is a very important region in our discussions. Therefore, for the region near zero bias we have analyzed only the G-V curves and we have calculated $(d\ln I/d\ln V)$ only outside the gap region.

[16] E. L. Wolf, *Principles of Electron Tunneling Spectroscopy* (Oxford University Press, New York, 1985).

[17] J. Y. T. Wei, N.-C. Yeh, and R. P. Vasquez, Phys. Rev. Lett. **79**, 5150 (1997).

[18] Masoud Sarvestani, Michael Schreiber, and Thomas Vojta, Phys. Rev. B **52**, R3820 (1995), and references therein.